Chemical equilibrium description of stable and metastable defect structures in *a*-Si:H

Gerhard Schumm*
Xerox Palo Alto Research Center, 3333 Coyote Hill Road, Palo Alto, California 94304
(Received 9 August 1993)

A model for the equilibrium and metastable defect structure in *a*-Si:H is presented. Allowing chemical equilibration between dangling bonds and weak bonds with a broadened band of available defect energy levels, and requiring electronic occupancy according to occupation statistics during the chemical equilibration process, an expression for the steady-state defect structure under general nonequilibrium conditions is derived. A single reaction involving *e*-*h* pair recombination is found to account for the vast majority of experimental data, such as the dependence of equilibrated and saturated defect densities on temperature, generation rate, and band gap. The model predicts an excess of charged defects in as-grown undoped *a*-Si:H and a change in the energetic distribution of defect states by light soaking with an associated decrease of the ratio of charged-to-neutral defects, in agreement with measurements.

I. INTRODUCTION

As the defect structure and metastable defect formation in amorphous silicon (*a*-Si:H) is of vital importance for device applications, in the past years considerable effort has been put into understanding the defect formation mechanisms. It is now experimentally well established that the defect density in both doped and undoped *a*-Si:H can be described by a chemical-type equilibrium reaction between intrinsic defects, the dangling bonds, and defect-free coordinations, the Si-Si or Si-H bonds.[1-5]

Equilibration in combination with a statistical energy distribution of potential defect sites,[6] generally known as the defect pool concept, has been very successful in describing not only the defect density but also the different defect distributions observed in *n*-type vs *p*-type material.[7,8] Because in doped material one defect charge state dominates, out of three possible basic equilibrium reactions

$$\text{Si-Si} \rightleftharpoons D^0 , \quad e + \text{Si-Si} \rightleftharpoons D^- , \quad h + \text{Si-Si} \rightleftharpoons D^+ ,$$

only the one creating D^+, in *p*-type material, or D^-, in *n*-type material, may be considered and the derivation of the defect density and distribution in this material is comparably straightforward. With the assumption that D^0 states dominate in undoped material, the density and temperature dependence of the neutral defect density were derived from the first reaction[4] along the same lines as in doped material. This assumption, however, is not necessarily valid, and in a first approach, applying the three simultaneous, but uncoupled, reactions for all three charge states, the defect structure in undoped material was derived.[9] There it was shown that the two charged defect bands observed in doped *a*-Si:H will also dominate the defect structure of undoped *a*-Si:H, if the basic structural parameters, defect pool width and effective correlation energy of the dangling bond (DB), which have been used to explain the energy positions of defect bands in doped material,[8] are also valid for undoped material.

Here we explore in more detail a generalized concept for the above reactions that has been introduced recently[10-12] and can be applied to both doped and undoped material in thermal equilibrium as well as under general nonequilibrium steady-state conditions such as light soaking, charge injection, or reverse bias annealing. By coupling the different reactions via electronic reoccupation during the chemical equilibration processes, it is shown that each of these reactions yields the same results for the defect distribution of equilibrated *a*-Si:H. This is in fact expected for true thermodynamical equilibrium, because the principle of detailed balance requires that all reactions that may occur satisfy equilibrium separately. Under nonequilibrium conditions, however, this is not the case. Different feasible reactions will give different results for metastable defect densities and distributions, and those reactions with the lowest-energy barrier will dominate the determination of metastable defect structures.

II. THEORETICAL FRAMEWORK

A. Thermodynamical equilibrium

Consider first the most simple chemical reaction where a weak Si-Si bond with electronic energy E_t breaks into two neutral dangling bonds at energy positions E_1 and E_2 in the gap[13]

$$\text{WB} \rightleftharpoons (D_1^0 + D_2^0)_{\text{pair}} , \tag{1}$$

where WB denotes weak bond. If no reactions involving free carriers and other charge states occur and no electronic reoccupation of the formed neutral defects takes place, the law of mass action for the neutral dangling-bond density is written

$$\frac{[D_1^0 + D_2^0]_{\text{pair}}}{[\text{WB}]} = \frac{(N_{D^0})_{\text{pair}}}{N_t - (N_{D^0})_{\text{pair}}} = \exp\left[-\frac{\Delta G}{kT}\right] , \tag{2}$$

where ΔG is the free energy of formation of the defect pair and N_t is the density of WB's before any are converted to defects. This is one of the basic reactions used in

Ref. 4 to explain the thermal equilibrium defect density in undoped material.

A number of other conversion mechanisms involving the same structural reconfiguration but different carriers and charge states may occur simultaneously to reaction 1:

$$\mathrm{WB} \rightleftharpoons (D_1^+ + D_2^-)_{\mathrm{pair}} , \tag{3}$$

$$e + \mathrm{WB} \rightleftharpoons (D_1^0 + D_2^-)_{\mathrm{pair}} , \tag{4}$$

$$h + \mathrm{WB} \rightleftharpoons (D_1^0 + D_2^+)_{\mathrm{pair}} , \tag{5}$$

$$e + h + \mathrm{WB} \rightleftharpoons (D_1^0 + D_2^0)_{\mathrm{pair}} . \tag{6}$$

(In Appendix A we generalize these reactions to include contributions by Si-H bonds.) More important, electronic reoccupation of the defects that are created neutral in reaction 1, such as $e + D^0 \rightleftharpoons D^-$, $h + D^0 \rightleftharpoons D^+$, occurs on much shorter time scales than structural equilibration. To account, for instance within reaction 1, for electronic reoccupation and all potential other reactions, the weak-bond concentration on the left-hand side of reaction 1 may be simply defined by subtracting the total, instead of the neutral, density of formed defects from the original weak-bond density N_t. In steady state, the neutral defect concentration on the right-hand side is given by equilibrium electronic occupancy statistics, $[D_1^0] = f^0(E_1)[D_1]$, $[D_2^0] = f^0(E_2)[D_2]$, and therefore $[D_1^0 + D_2^0]_{\mathrm{pair}} = f^0(E_1) f^0(E_2)[D_1 + D_2]_{\mathrm{pair}}$.

The law of mass action applied to reaction 1 then yields the total instead of only the neutral defect density

$$\frac{[D_1^0 + D_2^0]_{\mathrm{pair}}}{[\mathrm{WB}]} = \frac{(N_{D0})_{\mathrm{pair}}}{N_t - (N_D)_{\mathrm{pair}}} = \frac{f^0(E_1) f^0(E_2)(N_D)_{\mathrm{pair}}}{N_t - (N_D)_{\mathrm{pair}}} = \exp\left[-\frac{\Delta G}{kT} \right] , \tag{7}$$

with the single occupation probability $f^0(E)$ given by [14]

$$f^0(E) = \frac{2}{Z} \exp \frac{E_F - E}{kT} . \tag{8a}$$

The functions of zero occupancy, f^+, and double occupancy, f^-, needed below, are

$$f^+(E) = \frac{1}{Z} , \tag{8b}$$

$$f^-(E) = \frac{1}{Z} \exp \frac{2E_F - 2E - U}{kT} , \tag{8c}$$

where

$$Z = 1 + 2 \exp \frac{E_F - E}{kT} + \exp \frac{2E_F - 2E - U}{kT} .$$

The free energy of formation of the defect pair, ΔG, is determined by the reaction enthalpy ΔH and the change in entropy ΔS, $\Delta G = \Delta H - T\Delta S$.[15] With $\Delta S = k \ln 4$, due to the degeneracy factors of the two formed neutral DB's, the free energy of formation in Eq. (7) is

$$\Delta G = E_1 + E_2 - 2E_t - kT \ln 4 . \tag{9}$$

Here it is assumed that the reaction enthalpy can be approximated by the difference between the involved one-electron states of the DB's, E_1 and E_2, and of the weak bond, $2E_t$. With ΔG from Eq. (9), we get the total defect density from Eq. (7),

$$\frac{(N_D)_{\mathrm{pair}}}{N_t - (N_D)_{\mathrm{pair}}} = \frac{2}{f^0(E_1)} \frac{2}{f^0(E_2)} \exp \left[-\frac{E_1 + E_2 - 2E_t}{kT} \right] \tag{10a}$$

or

$$(N_D)_{\mathrm{pair}} = \frac{N_t}{1 + \frac{f^0(E_1)}{2} \frac{f^0(E_2)}{2} \exp \left[\frac{E_1 + E_2 - 2E_t}{kT} \right]} . \tag{10b}$$

The physical mechanism leading to a larger defect density in Eqs. (7) and (10) as compared to Eq. (2) is the depletion of created neutral defects on the right-hand side of the chemical equilibrium reaction (1) by electronic reoccupation to charged defects. This depletion requires the conversion of additional WB's to maintain the equilibrium determined by the law of mass action between WB's and neutral DB's, and therefore increases the total number of defects.

B. Other defect reactions

Because electronic reoccupation of the defects that are initially formed in a particular charge state couples all potentially occurring structural reactions, according to detailed balance in equilibrium each of the other reactions, Eqs. (3)–(6), should yield the same results for the total defect density. Consider, for instance, reaction 4, $e + \mathrm{WB} \rightleftharpoons (D_1^0 + D_2^-)_{\mathrm{pair}}$. The law of mass action gives

$$\frac{[D_1^0 + D_2^-]_{\mathrm{pair}}}{[e][\mathrm{WB}]} = \frac{f^0(E_1) f^-(E_2)(N_D)_{\mathrm{pair}}}{n_0 (N_t - (N_D)_{\mathrm{pair}})} = \exp \left[-\frac{\Delta G}{kT} \right] \tag{11}$$

with the free electron density

$$n_0 = N_c \exp \left[\frac{E_c - E_F}{kT} \right] \tag{12}$$

and the free energy difference

$$\Delta G = \Delta H - T\Delta S = (E_1 + 2E_2 + U) - (2E_t + E_c) - kT(\ln 2 - \ln N_c) . \tag{13}$$

Here, ΔH is the difference between the sums of one-electron states on the left- and right-hand sides of reaction 4. The entropy change is determined by the degeneracy of the neutral DB state, which is 2, and the degeneracy of the free electron in the conduction band, which is N_c.[16] With Eqs. (12) and (13), Eq. (11) becomes

$$\frac{(N_D)_{\text{pair}}}{N_t-(N_D)_{\text{pair}}}=\frac{2}{f^0(E_1)}\frac{1}{f^-(E_2)}\exp\left[\frac{E_F-U-E_2}{kT}\right]\times\exp\left[-\frac{E_1+E_2-2E_t}{kT}\right]. \quad (14)$$

The first exponential is due to the change in reaction enthalpy, $E_F-(E_2+U)$, when forming a D^- instead of D^0 state by taking an electron from the Fermi level into the D^- state at E_2+U. Using the expression for the equilibrium occupation functions, Eq. (8), it is easy to show that Eq. (14) is identical to Eq. (10). In the same way, it can be shown that all the other listed reactions will yield a result for the defect density that can be converted into Eq. (10). These results demonstrate nicely that the change of formation energies for defects in different charge states, by dropping electrons onto or picking electrons from the Fermi level, is actually a result of shifting the equilibrium point in the reaction by reoccupation of defects created in a specific charge state.

A graphical representation of this coupling is attempted in Fig. 1. As an example we have depicted our four structural reactions, where WB's are converted into DB's of different charge states. At the same time we allow electronic equilibration between the different charge states. In equilibrium, it suffices that only one of the chemical reactions actually occurs, because in combination with electronic reoccupation all the other charge states can be accessed subsequently. And because in thermal equilibrium detailed balance applies, all reactions will lead to the same result regarding the defect density and charge states, as exemplified with reactions 1 and 4 above. Using occupation statistics, the description of equilibrium by three different reactions in n-doped, p-doped, and undoped material becomes obsolete (and in fact is incorrect). In reality, only one chemical reaction may be possible, for instance, the reaction involving e-h pair recombination, while the kinetic barrier for the other listed reactions may be too high. This reaction determines then the defect structure in both undoped and doped material. However, because all reactions yield identical results for the equilibrium defect structure, in equilibrium there is no way of telling which reaction actually drives defect creation.

In equilibrium, the splitting of the conversion process into a chemical reaction and subsequent electronic reoccupation may appear artificial. This splitting, however, is essential in the nonequilibrium steady-state case, because, using the nonequilibrium steady-state occupancy functions instead of the equilibrium ones, the results from the different reactions can no longer be converted into each other. The various potential reactions will give different results regarding the metastable defect density and distribution. We will discuss this in more detail in Sec. II D.

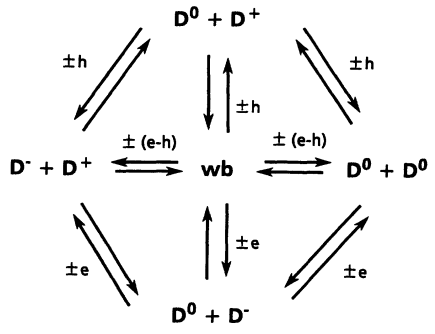

FIG. 1. Chemical reactions, indicated by radial arrows, and electronic reoccupation, indicated by the circular arrows.

C. Energy distribution of weak Si-Si bonds and available defect sites

The amorphous nature of the silicon network, with bond angle and bond length fluctuations, leads to an exponential distribution of weak Si-Si bond energies with an exponential slope kT_v,

$$g(E_t)=N_{v0}\exp\left[-\frac{E_t}{kT_v}\right] \quad (15)$$

and to a broadened band of energy levels available for creation of potential defect states. For convenience we assume a Gaussian spreading of E_1 and E_2 according to

$$P(E)=\frac{1}{\sqrt{2\pi}\sigma}\exp-\frac{(E-E_p)^2}{2\sigma^2} \quad (16)$$

($E=E_1$ or E_2), with a rms bandwidth σ and a most probable energy position or pool center E_p.

The equilibrium reactions of Sec. II A may now be treated differentially. By detailed balance, each subset of weak bonds, d^3N_t, must be in equilibrium with each subset of DB's at E_1 and E_2, as indicated in Fig. 2. Equation (10) is then

$$d^3(N_D)_{\text{pair}}=\frac{d^3N_t}{1+\frac{f^0(E_1)}{2}\frac{f^0(E_2)}{2}\exp\left[\frac{E_1+E_2-2E_t}{kT}\right]}, \quad (17)$$

where d^3N_t is the subset of those weak bonds at E_t that may be converted to a DB at E_1 and the other DB at E_2,

$$d^3N_t=g(E_t)P(E_1)P(E_2)dE_t dE_1 dE_2 . \quad (18)$$

To solve for the gap-state density at E_1 or E_2, $d^3(N_D)_{\text{pair}}$ must be integrated over the respective other two variables, e.g.,

$$D_{\text{pair}}(E_2)=\int_{E_1}\int_{E_t} d^3(N_D)_{\text{pair}}dE_t dE_1 , \quad (19)$$

with $d^3(N_D)_{\text{pair}}$ given by Eqs. (17) and (18). Since each conversion produces two DB's, and the reaction is symmetrical with respect to the subscripts 1 or 2, the total defect density is $D(E)=2D_{\text{pair}}(E)$. Integrating over $E_1=-\infty,\ldots,+\infty$ and suitably rearranging, we find an analytical solution with no approximations,

$$D(E)=\gamma P(E+\sigma^2/2kT_v)\left[\frac{2}{f^0}\right]^{T/2T_v} . \quad (20)$$

Equation (20) is the central expression for the equilibrium

defect density and distribution in a-Si:H.[10,11] The physical mechanisms leading to the various terms are discussed in Sec. III A. The scaling factor γ contains the parameters T, kT_V, E_p, σ, U, and, in the case of H-mediated defect reactions, the hydrogen density N_H. For an extension of the structural reactions including Si-H bonds, and a derivation of γ, see Appendix A.

D. Metastable defect structure

There is general agreement that the metastable defect structure and density achieved under nonequilibrium conditions is closely related to the electron and/or hole concentrations induced by these conditions. To derive the metastable defect structures, we make three basic assumptions.

(1) The chemical reactions that control the defect structure in equilibrium will also determine the defect structures obtained under nonequilibrium conditions.

(2) The only effect of a nonequilibrium situation such as light soaking, carrier injection, or carrier depletion, is to change the free electron and hole concentrations and, as a result of that, the steady-state occupancy of the defects.

(3) Under nonequilibrium conditions, a new steady state for the metastable defect structure may be reached.

The appropriate reactions identified as driving the defect formation may then be treated in analogy to Sec. II B by the law of mass action, but now using the nonequilibrium concentrations for charge carriers and the associated nonequilibrium occupancy functions. A formal justification for such a treatment is given in Appendix B. Reactions 1 and 3 are independent of the electron and hole concentration and therefore may be ruled out as driving metastable defect creation. If electron and/or hole trapping drives the chemical reaction, reactions 4 and/or 5 apply. If e-h pairs initiate the conversion process, reaction 6 applies.

Electron-hole recombination. The law of mass action for reaction 6 yields

$$\frac{[D_1^0+D_2^0]_{\text{pair}}}{[e][h][\text{WB}]}=\frac{f^{0*}(E_1)f^{0*}(E_2)(N_D)_{\text{pair}}}{np\,[N_t-(N_D)_{\text{pair}}]}=\exp\left[-\frac{\Delta G}{kT}\right], \tag{21}$$

where

$$\Delta G=\Delta H-T\Delta S=(E_1+E_2)-(2E_t-E_g)-kT(\ln 2-\ln N_c N_v)\ ,$$

and

$$f^{0*}(E,n,p)=\frac{1}{1+\dfrac{e_n^0+pc_p^0}{e_p^++nc_n^+}+\dfrac{e_p^0+nc_n^0}{e_n^-+pc_p^-}} \tag{22}$$

is the nonequilibrium occupancy function[17] with the capture coefficients of electrons and holes into charged and neutral traps, c_n^0, c_p^0, c_p^-, and c_n^+, and the associated emission coefficients, e_n^0, e_p^0, e_n^-, and e_p^+. (Similar expressions apply for zero and double occupancy, f^{+*} or f^{-*}). With $n_0p_0=N_cN_v\exp[-E_g/kT]$ one gets from Eq. (21)

$$\frac{(N_D)_{\text{pair}}}{N_t-(N_D)_{\text{pair}}}=\frac{2}{f^{0*}(E_1)}\frac{2}{f^{0*}(E_2)}\times\exp\left[-\frac{E_1+E_2-2E_t}{kT}\right]\frac{np}{n_0p_0} \tag{23}$$

and, by differential treatment, the metastable steady-state density of states

$$D_{\text{SS}}(E)=\gamma_i^*P(E+\sigma^2/2kT_v)\left[\frac{2}{f^{0*}}\right]^{T/2T_v}\times\left[\frac{np}{n_0p_0}\right]^{\rho T/2T_v}, \tag{24}$$

with $\rho=(1+iT/2T_v)^{-1}$ if $i=0$, 1, or 2 Si-H bonds are involved (see Appendix A). Equation (24) bears close similarity to the expression for the equilibrium case, Eq. (20), except that $(2/f^0)$ is replaced by $(2/f^{0*})$, and $D_{\text{SS}}(E)$ is larger than $D(E)$ by the deviation of the np product from equilibrium, $[np/n_0p_0]^{\rho T/2T_v}$. The scaling factor γ_i^* is essentially the same as γ_i of Eq. (A6), but f^0 in the integral (A8) is replaced by f^{0*}.

Electron or hole trapping. Proceeding the same way for the reaction involving a single electron, one obtains

$$D_{\text{SS}}(E)=\gamma_i^*P(E+\sigma^2/2kT_v)\left[\frac{2}{f^0}\frac{f^-}{f^{-*}}\right]^{T/2T_v}\times\left[\frac{n}{n_0}\right]^{\rho T/2T_v} \tag{25}$$

and an analogous expression for involvement of a single hole. γ_i^* in Eq. (25) is the same as in Eq. (24).

With electron or hole trapping driving defect formation, the enhancing factor for the resulting metastable defect density is smaller than with e-h pair recombination. For e-h recombination, the deviation of the e-h product from equilibrium, np/n_0p_0, is the driving force, whereas for e or h trapping only the deviation of single carrier densities, n/n_0 or p/p_0, enters the associated laws of mass action, which is a smaller number. As shown in the next section, not only the magnitude but also the spectral shape of $D_{\text{SS}}(E)$ is now dependent on the specific reaction involved, and, unlike in the equilibrium situation, the results for $D_{\text{SS}}(E)$ based on the different reactions cannot be converted into each other.

III. MODEL RESULTS

The analytical expressions for $D(E)$ and $D_{\text{SS}}(E)$ give the spectral shape and the total defect density as a function of experimentally well-known and accessible structural parameters inherent to a-Si:H, and may be used for a critical testing of the underlying equilibration model and specific reactions.

A. Spectral shape in equilibrium

The spectral shape of $D(E)\sim P(E+\sigma^2/2kT_v)(2/f^0)^{T/2T_v}$ does not depend on the scaling factor γ and is

determined only by the structural parameters' pool position E_p, defect band broadening σ, tail slope kT_v, and, through Eq. (8), the correlation energy U and Fermi energy E_F. $P(E+\sigma^2/2kT_v)$ is a Gaussian. It has the same width as the defect pool, but centered at $\sigma^2/2kT_v$ below the pool position E_p.

The essential difference of Eq. (20) to the result of Ref. 4 is the additional factor $(2/f^0)^{T/2T_v}$. According to Eq. (8a), the neutral occupation probability is $f^0(E,E_F,U)\approx 1$ in the range $[E_F-U,E_F]$ and tails off exponentially with slope kT outside. Then, $(2/f^0)^{T/2T_v}$ is constant and close to 1 in the range $[E_F-U,E_F]$ and increases exponentially with slope $2kT_v$ outside. This factor produces the two charged sidebands shown in Fig. 2, a band of D^+ states above E_F and a band of D^- states below E_F, at the positions indicated in the figure. The physical mechanism responsible for the formation of the sidebands is the depletion of created neutral defect states by subsequent reoccupation to charged defects. This depletion drives the simultaneously occurring chemical equilibrium reaction towards the right. Because reoccupation occurs selectively outside the range $[E_F-U,E_F]$, it causes formation of additional defects preferentially below E_F-U and above E_F, therefore forming the two sidebands observed.

For the calculations here and in the following figures we have adopted a set of standard parameters typical for high-quality a-Si:H which are summarized in Table I. The parameters U and σ are less well known, and their effect on the spectral distributions is studied in detail below. Their effect on the integrated defect density, however, is rather small.

The bands in Fig. 2 are found to be of width σ, identical to the width of the pool distribution $P(E)$. Equation (20) produces the D^+ band at the same position as the pool distribution, consistent with a formation energy of D^+ states that is independent of their energetic position in the gap.[8] The D^0 band is located below the pool position E_p, because the formation energy for singly occupied defects increases with their position in the gap, $\Delta H^0\sim E_{D0}$, due to the promotion of an electron into the defect. Free energy minimization in combination with a distribution of weak-bond energies then yields the peak at $\sigma^2/2kT_v$ below E_p. Similarly, the $+/0$ transition of the

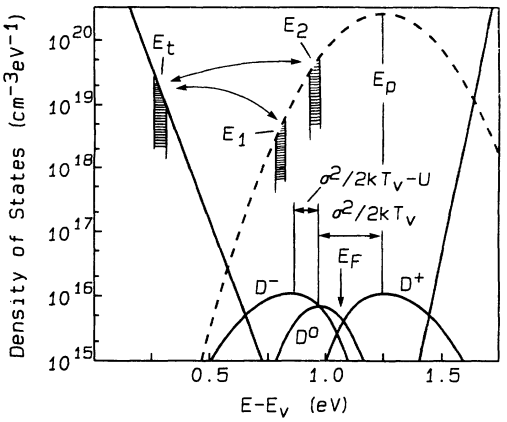

FIG. 2. Chemical equilibrium reaction between subsets d^3N_t, d^3N_{D1}, and d^3N_{D2}, and resulting defect bands. Instead of plotting the one-electron density of states, i.e., the $+/0$ transition levels of $D(E)$ (as done in Fig. 4), the bands are plotted according to actual occupancy in dark equilibrium, a band of D^0, D^+, and D^- states: $D^0(E)=f^0(E)D(E)$, $D^+(E)=f^+(E)D(E)$, and $D^-(E+U)=f^-(E)D(E)$ where $D(E)$ is given by Eq. (20).

D^- band is shifted twice as much towards lower energies than the D^0 band, because the formation energy for D^- defects includes the promotion of two electrons into the associated defect states, $\Delta H^-\sim 2E_{D0}$. Again, these results demonstrate that the concept of different formation *energies*, depending on the charge state of the final defects, is equivalent to changing formation *probabilities* due to the reoccupation of created defects.

A comparison with Ref. 4 shows that the shift of the D^0 and D^- band away from the pool center is only half as much as in their derivation. The reason for this smaller shift is that in Ref. 4 the two DB's in each reaction are assumed to form at the same energy position, while the above treatment allows statistically independent energy positions for each of the two DB's (see also Appendix A).

To satisfy charge neutrality, in undoped material the D^+ and D^- bands must be of equal density. Hence charge neutrality in combination with Eq. (20) relates E_F to the structural parameters, E_p, σ, kT_v, and U, and one gets for undoped a-Si:H

TABLE I. Standard set of parameters used for calculation of defect distributions. Capture rates from Ref. 26. VB denotes valence band.

Valence-band tail slope	kT_v	45 meV
Freeze-in temperature	T	190°C
Density of states at VB edge	N_{v0}	10^{21} cm^{-3} eV^{-1}
Hydrogen concentration	N_H	5×10^{21} cm^{-3}
Band gap	E_g	1.75 eV
Fermi level (with respect to VB edge)	E_F	1.05 eV
Correlation energy	U	0.15 eV
Pool width	σ	157 meV
Capture rates	c_n^0	1×10^{-8} cm^3 s^{-1}
	c_n^+	5.5×10^{-8} cm^3 s^{-1}
	c_p^0	1.1×10^{-9} cm^3 s^{-1}
	c_p^-	2.7×10^{-9} cm^3 s^{-1}

$$E_F = E_p - \frac{\sigma^2}{2kT_v} + \frac{U}{2} \quad . \tag{26}$$

In doped material, E_F is shifted away from this position and either the D^- band, in n-type material, or the D^+ band, in p-type material, dominates while the other two bands are quenched, as shown in Fig. 3. However, according to Eq. (20) and Figs. 2 and 3 the *positions* of the defect bands depend little on doping provided that the basic structural parameters, pool position, pool width, valence-band tail slope, and correlation energy, do not change strongly. The band positions in doped material are well known. In p-type a-Si:H a band of D^+ defects with the $D^{+/0}$ transition at $E_c - 0.55$ eV and in n-type material a band of D^- defects with a $D^{-/0}$ transition at $E_c - 0.95$ eV is generally observed, giving an energetic spacing $E_{D^+} - E_{D^-} \sim 0.4$ eV.[18–20] Knowing the band positions in n- and p-type material from experiment, we take into account only pairs of U and σ that give the observed spacing

$$E_{D^+} - E_{D^-} = \sigma^2/kT_v - U \sim 0.4 \text{ eV} \quad . \tag{27}$$

If we assume a typical defect bandwidth $\sigma \sim 150$–180 meV and a tail slope $kT_v = 45$ meV for device-quality a-Si:H, a correlation energy $U \sim 0.1$–0.3 eV is required to obtain the observed spacing. Both Figs. 2 and 3 were calculated using $U = 0.15$ eV and $\sigma = 157$ meV, but other U-σ pairs that satisfy Eq. (27) give very similar results.

In undoped a-Si:H, two defect bands are observed, incidentally located at the same positions as found in doped material,[20–23] but the assignment to particular transition levels so far has been ambiguous.[21,23] In principle there are two options. The first option is that the two defect bands observed at $E_c - 0.95$ eV and $E_c - 0.55$ eV are the $+/0$ and $0/-$ transition levels of the same defect, and in dark equilibrium most defects will be neutral This assignment is the widely accepted standard defect model for undoped a-Si:H. It requires a discrete change in structural properties going from doped to undoped material. In particular, a larger U than in doped material, $U \sim 0.4$ eV, a smaller σ, and a different pool position to account for the changed energy positions of the transition levels, apply. The other option is that the structural parameters U, σ, and E_p found in n- and p-type material determine the defect structure of undoped a-Si:H as well. Then the two defect bands in undoped a-Si:H are those observed separately in either p- or n-type material, but now are both present in equal density to satisfy charge neutrality. This assignment is predicted by the defect pool model.[6,9,24] In this case, in the dark a large fraction of the defects are charged, such as is found in Fig. 2.

The two defect structures according to the standard and defect pool models are both given by Eq. (20) and compared in Fig. 4. For the calculations we have applied the set of standard parameters, given in Table I. Shown is the one-electron density of states $D(E)$, i.e., the $+/0$ transition levels given by Eq. (20). With an assumed $U = 0.15$ eV and $\sigma = 157$ meV, identical to the doped material, the defect pool structure in the lower part of the figure is obtained. Actual occupancy in the dark yields the three defect bands plotted in Fig. 2 where the two charged defect bands are formed at $E_F \pm 0.2$ eV, the D^+ band at $E_c - 0.55$ eV and the D^- band at $E_c - 0.95$ eV. With a larger $U = 0.4$ eV and smaller $\sigma = 120$ meV, on the other hand, the standard defect structure in the upper part of Fig. 4 is formed.

It is highly unlikely that the basic structural properties of the a-Si network, determining the correlation energy and the statistically most probable position E_p for defect states, are the same for p- and n-type material and do not depend on the doping level over orders of magnitude, but do change discretely when going from undoped to doped material. There are, further, a number of inconsistencies relating the standard defect model to experimental observations.[9,24] In the remainder of the paper we therefore

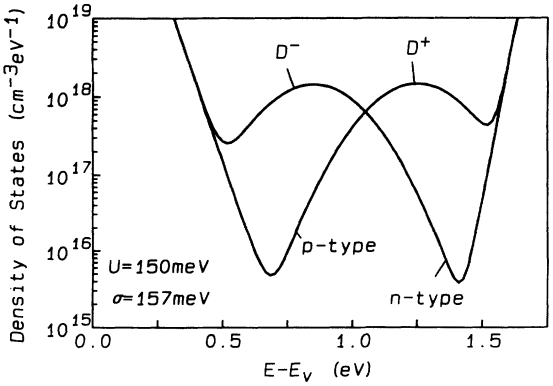

FIG. 3. Density of states in doped a-Si:H according to Eq. (20), assuming $E_F = E_v + 0.55$ eV in p-type, and $E_F = E_c - 0.3$ eV in n-type material. The D^- band in n-type a-Si:H has been shifted by the correlation energy U.

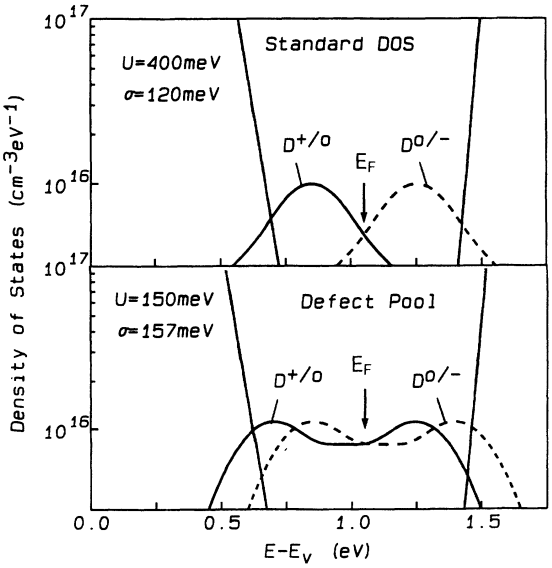

FIG. 4. Standard defect structure with $E^{-/0} - E^{0/+} = 0.4$ eV, and defect pool distribution where in dark equilibrium $E_{D^+} - E_{D^-} = 0.4$ eV. Full lines denote the one-electron density of states (DOS) given in Eq. (20), dashed lines denote the corresponding two-electron DOS shifted by the correlation energy.

focus on the assignments given by the defect pool model.

It is illustrative to calculate from Eq. (20) the defect distribution and corresponding ratio R of charged-to-neutral defects in the dark for a given spacing $E_{D^+}-E_{D^-}$ as a function of the less well-known U [and corresponding σ according to Eq. (27)] where

$$R=\frac{N_{D^+}+N_{D^-}}{N_{D^0}}=\frac{\int[f^+(E)+f^-(E)]D(E)dE}{\int f^0(E)D(E)dE}\ .$$

The results are shown in Figs. 5 and 6. Maintaining $E_{D^+}-E_{D^-}\sim 0.4$ eV, the three defect structures in Fig. 5 look very similar. The positions for the charged bands, D^- and D^+, are fixed at $E_F\pm 0.2$ eV, only the D^0 band shifts, according to $E_{D0}=E_F-U/2$, and increases in comparison to the charged bands. According to Eq. (27), σ increases only by $\sim 25\%$ for U from 0.1 to 0.4 eV. For $U\sim 0.2$ eV (and corresponding $\sigma\sim 164$ meV) the charged defect density exceeds the neutral defect density by a factor 4, but even for $U\sim 0.4$ eV ($\sigma\sim 190$ meV) by a factor 2 more charged defects are found, indicating that charged defects cannot be neglected in undoped annealed a-Si:H.

It should be noted that these are very general results that depend little on the particular model involved. For a given spacing $E_{D^+}-E_{D^-}$, the approach where both defects in the reaction are produced at the same energy,[9,12] or even the simple approach with no distribution of precursor energies,[25] yield almost identical charged-to-neutral ratios as a function of U, with only somewhat smaller corresponding σ's required to maintain the same $E_{D^+}-E_{D^-}$.

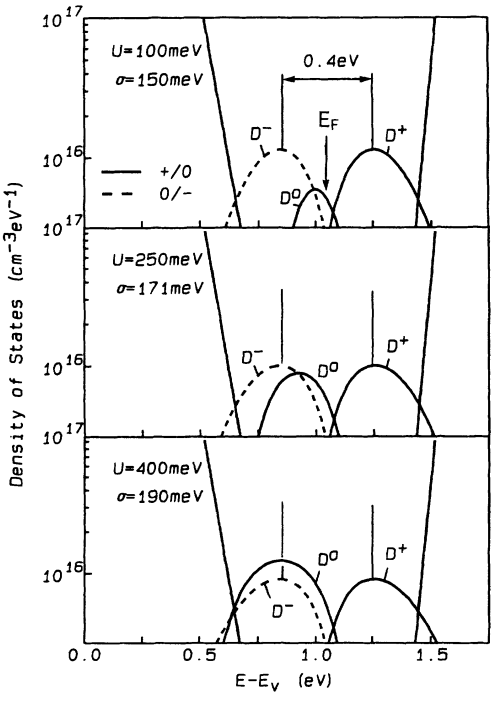

FIG. 5. Defect pool distribution separated into bands D^-, D^0, D^+ as occupied in the dark, for various U and corresponding σ to maintain a given spacing $E_{D^+}-E_{D^-}=0.4$ eV. Full and dashed lines denote one- and two-electron DOS's respectively.

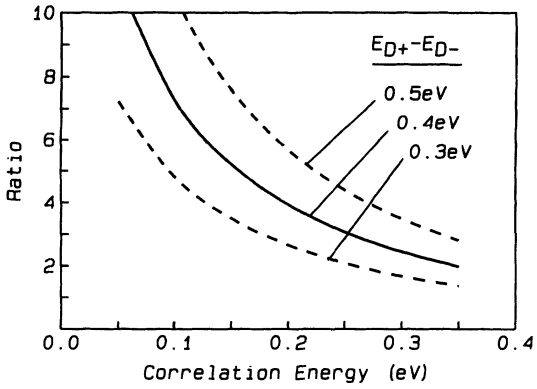

FIG. 6. Ratio of charged-to-neutral defects, resulting from defect structures shown in Fig. 5, as a function of U, for various given spacings $E_{D^+}-E_{D^-}$.

B. Spectral shape of light-induced defects

As already pointed out, the energetic distribution of nonequilibrium defect states may deviate substantially from the established equilibrium structure. Under illumination the system drives towards a new steady-state defect distribution described by Eq. (24) or (25), depending on whether e-h recombination or single carrier trapping drives defect creation. In order to calculate $D_{SS}(E)$, where the non-equilibrium occupancy function $f^*(E,n,p)$ is given by Eq. (22), we need in addition to the structural parameters in Table I the electron and hole densities under illumination as well as the various capture rates. For the following figures we use capture rates from double injection experiments[26] given in Table I, an electron density $n=10^{13}$ cm^{-3} corresponding to typical photoconductivities around 10^{-5} Ω^{-1} cm^{-1} observed on degraded samples under strong illumination, and $p=n/10$ as determined from steady-state $\mu\tau$ measurements.[27]

Electron-hole recombination. Figure 7 shows the equilibrium and light-induced defect distribution according to Eqs. (20) and (24) for the set of standard parameters, assuming that e-h pair recombination drives the defect creation. The gap states show largest growth in the midgap range with a particularly strong increase of the D^0 band. From Eq. (22) it can be shown that the nonequilibrium occupancy $f^{0*}(E)$ is nearly constant between the quasi Fermi levels $[E_{Fp},E_{Fn}-U]$. Therefore the formation of the two sidebands, which in equilibrium was caused by selective reoccupation of created neutral defects during chemical equilibration in the region outside $[E_F-U,E_F]$, is now largely suppressed between the quasi Fermi levels, which typically is a much larger range. The peak of the light-soaked defect structure is located at the same position as the neutral defect band in annealed material. It should be pointed out that the two smaller charged sidebands in the figure were created as neutral defects as a result of e-h pair recombination and not by e

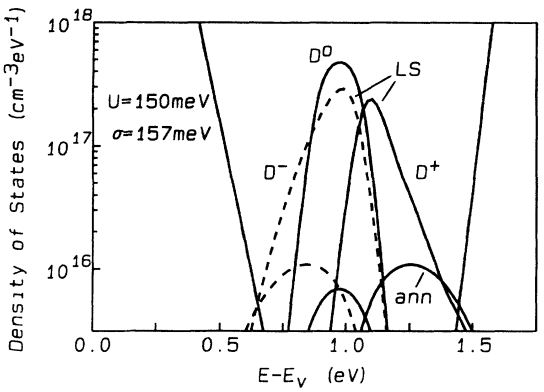

FIG. 7. The defect structure of light-soaked and equilibrated a-Si:H, according to Eqs. (24) and (20). The bands are shown as occupied in dark equilibrium.

or h trapping. Reoccupation according to dark occupation statistics yields these sidebands only in the dark after light soaking.[10] Depending on the ratios of free electron to hole densities, asymmetries in the nonequilibrium occupation functions and quasi Fermi levels yield asymmetries in the spectral shape of the defect structure. For $n>p$, more defects are formed below $E_p-\sigma^2/2kT_v$ than above $E_p-\sigma^2/2kT_v$. Charge neutrality causes then a lower position of E_F in light-soaked material, which may explain the generally observed shift of E_F towards midgap with light soaking. With the above parameters a shift of E_F by 30 meV is found; other parameters yield up to 80 meV.

Integrating the defect bands for the set of standard parameters one finds that by light soaking the ratio of charged-to-neutral defects drops from $R_{\rm ann}\sim 5$ to $R_{\rm LS}\sim 1.5$. Figure 8 shows $R_{\rm ann}$ and $R_{\rm LS}$ as a function of U for a given spacing $E_{D^+}-E_{D^-}=0.4$ eV. For all values of U, $R_{\rm LS}$ is found comparably small, $\sim 0.5-1.5$, indicating that, unlike in annealed material, in light-soaked a-Si:H the density of charged defects does not significantly exceed the density of the neutral defects.

The decrease of R with light soaking is a prediction

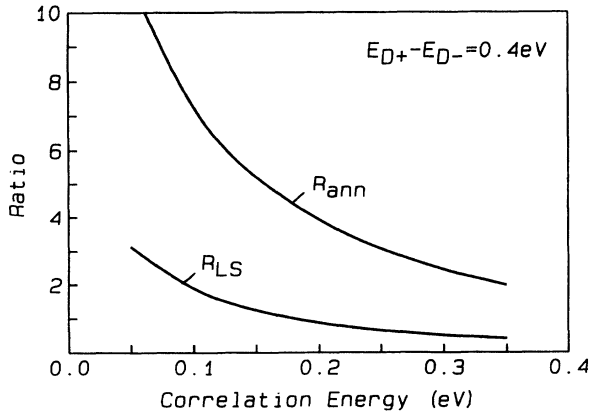

FIG. 8. Ratio of charged-to-neutral defects. $R_{\rm LS}$ for light-soaked defect structures, $R_{\rm ann}$ for equilibrated defect structures, as a function of U.

that may be directly tested by comparing subgap absorption with spin density on very thick films. Making the usual assumption that D^0 states have two spectral contributions to a photothermal deflection spectrum (PDS), one by promotion of an electron from the valence band into D^0, the other by promotion of an electron from D^0 into the conduction band, the integrated subgap absorption is $\alpha\sim N_D^+ + N_D^- + 2N_{D^0}$, and the ratio of subgap absorption to spin density is $(N_{D^+}+N_{D^-}+2N_{D^0})=R+2$. While both the calculated $R_{\rm ann}$ and $R_{\rm LS}$ drop by more than a factor 5 for U increasing from 0.1 to 0.4 eV, the experimentally accessible quantity $(R_{\rm ann}+2)/(R_{\rm LS}+2)$ turns out to depend little on the assumed correlation energy, decreasing slightly from 2.3 to 1.7 for $U=0.1-0.4$ eV. Therefore this quantity may provide a critical test of the model. Figure 9 shows subgap absorption vs spin density of three undoped high-quality a-Si:H samples[28,29] at various light-soaked stages. The data show a clear deviation from proportionality over the whole range up to saturation. The error bars reflect an uncertainty of $\pm 4\times 10^{12}$ spins, and are smaller for the light-soaked and for the thicker samples. Best fits were obtained for $(R_{\rm ann}+2)/(R_{\rm LS}+2)=2.3-2.0$, corresponding to $U\sim 0.1-0.2$ eV and $R_{\rm ann}\sim 4-7$. The lines shown in Fig. 9 are calculated for $(R_{\rm ann}+2)/(R_{\rm LS}+2)=2.3$.

While the experimental data do not prove the model, the agreement with predicted changes is excellent. Using $(R_{\rm ann}+2)/(R_{\rm LS}+2)=2.3$, for $R_{\rm LS}=0$ (no charged defects present after light soaking), a lower limit of the charged-to-neutral ratio in annealed material $R_{\rm ann}\simeq 2.6$ is obtained. $R_{\rm LS}=0.5$, corresponding to a fraction of 33% charged defects in light-soaked material, yields $R_{\rm ann}\simeq 4$. $R_{\rm LS}=1$, corresponding to 50% charged defects, yields $R_{\rm ann}\simeq 5$. These results demonstrate that the relatively small deviations from proportionality observed between subgap absorption and spin density can indicate and certainly are consistent with quite large ratios of

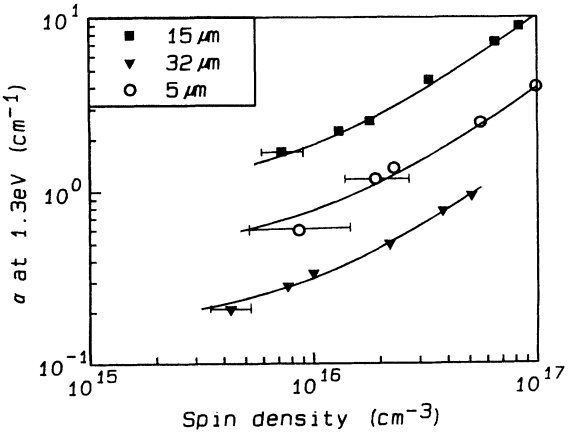

FIG. 9. Subgap absorption and spin density with light soaking. 15- and 32-μm films: Ref. 28; 5 μm film: Ref 19. Full lines according to $(R_{\rm ann}+2)/(R_{\rm LS}+2)=2.3$. All data follow essentially the same line. To allow for better discrimination, data associated with full symbols have been displaced by $\pm\log_{10}2$ on α axis.

charged-to-neutral defect densities in annealed *a*-Si:H.

Electron or hole trapping. Spectral shapes of the defect distribution with a single dominant defect band are also obtained assuming reactions that involve only electron or hole trapping, given by Eq. (25). The physical reason for obtaining a single defect band is again a constant occupation probability between the two quasi Fermi levels and therefore no depletion of created defects by selective reoccupation. The main difference to *e-h* pair recombination regarding the energy distribution is the position of these bands. While *e-h* pair recombination produces neutral defect states centered around the position of the D^0 band of annealed *a*-Si:H, $E_p-\sigma^2/2kT_v$, hole trapping produces initially positive charged defects around E_p and electron trapping creates initially negative charged defects around $E_p-\sigma^2/kT_v$. The difference in energy positions is explained by the different formation energies for positive and negative defects as compared to neutral ones. If electron or hole trapping were responsible for defect creation, because the bulk of defect states is created at positions away from the D^0 band of annealed *a*-Si:H, comparably large associated shifts of E_F with light soaking would be required to maintain charge neutrality in the dark. Electron trapping would produce shifts by 250 meV towards E_v, hole trapping would produce shifts towards E_c by 150 meV.

Another difference is found for the integrated defect *density.* While the reaction involving *e-h* pair recombination enhances the defect density by roughly a factor 10–20 (see Fig. 7) under typical light-soaking conditions, hole trapping increases the defects by a factor 5–10, and electron trapping would produce even a slight decrease. The reason for the reduced efficiency in creating metastable defects is the smaller term n/n_0 or p/p_0 as compared to np/n_0p_0 in the expression for the metastable defect structure.

Considering the smaller efficiency in producing light-induced defects and the predicted large shifts in defect positions with associated shifts in E_F, these reactions probably can be ruled out as being responsible for light-induced degradation of *a*-Si:H. Although available data on single carrier injection are not sufficient to completely discard these reactions for such conditions, we point out that the reaction involving *e-h* pair recombination implicitly accounts for single carrier injection as well, by setting in Eq. (24) either $n=n_0$ for hole injection or $p=p_0$ for electron injection. The predicted changes in defect density from such a reaction are in good agreement with experimental data.[30]

C. Integrated defect density

With $N_0=\int f^0(E)D(E)dE$ and using the standard set of parameters one obtains from Eq. (20) with the scaling factor γ_i the D^0 densities, $N_0\sim10^{12}$, $N_0\sim5\times10^{13}$, or $N_0\sim2\times10^{15}$ cm^{-3} for $i=0$, 1, or 2 Si-H bonds involved. These numbers depend little on the exact values of the input parameters, U, σ, etc. Comparison with experimentally observed spin densities $N_0\simeq10^{15}$ cm^{-3} suggests that the reaction involving two Si-H bonds, Eq. (A3), is driving the defect creation. This reaction also appears to be in agreement with microscopic arguments.[5] Therefore throughout the paper $i=2$ has been used to calculate the $D(E)$.

Equilibrium and saturated light-induced defect densities, N_{eq} and N_{sat}, are well characterized quantities in *a*-Si:H and have been correlated with various parameters. N_{eq} has been found to be thermally activated above the freeze-in temperature[4,5,31] and to be related to the valence-band tail slope.[32,33] N_{sat} has been correlated to the band gap,[33] tail slope,[33] hydrogen content,[33,34] generation rate,[35–37] and temperature.[35–37] So an extensive pool of experimental data is available to test the predictions of the model.

The equilibrium defect density is obtained by integration of Eq. (20).

$$N_{eq}=\int D(E)dE \ . \tag{28}$$

The saturated defect density may be calculated from Eq. (24),

$$N_{sat}=\int D_{SS}(E,n,p)dE \ , \tag{29}$$

where

$$n=G/c_nN_{sat} \ , \quad p=G/c_pN_{sat} \ . \tag{30}$$

Equation (30) is a crude approximation for free carrier densities and may be replaced by a more accurate recombination model,[17] but is sufficient for the present purposes.

D. Dependence on band gap and hydrogen concentration

Studies of samples with different band gaps and hydrogen content have indicated that the saturation defect density is smaller for lower hydrogen content and lower band gap.[33,34] Because E_g and c_H are also correlated, the experimental data do not permit discrimination between the effects on N_{sat} of these two parameters. The derived equation for $D_{SS}(E)$ suggests that both parameters play a role in determining N_{sat}. Regarding the dependence on E_g, from Eq. (24) one gets

$$N_{sat}\sim D_{SS}(E)\sim\left[\frac{np}{n_0p_0}\right]^{\rho T/2T_v} , \tag{31}$$

where $np\sim(G/N_{sat})^2$ and $n_0p_0\sim\exp(-E_g/kT)$.

Solving for N_{sat}, one finds

$$N_{sat}\sim\left[G\exp\left[\frac{E_g}{2kT}\right]\right]^{1/(1+T_v/\rho T)} \tag{32}$$

and with $kT_v=45$ meV, at room temperature,

$$\frac{d(\log_{10}N_{sat})}{dE_g}\sim3.06\text{eV}^{-1} \ , \ 2.59\ \text{eV}^{-1} \ , \ 2.24\ \text{eV}^{-1}$$

for $i=0$, 1, 2, respectively. Figure 10 shows the dependence of N_{sat} on E_g, calculated from Eq. (24) for $i=2$. In addition to the set of standard parameters given in Table I, a generation rate $G=4\times10^{22}$ cm^{-3}, close to the reported rates[33] used to produce the associated experimen-

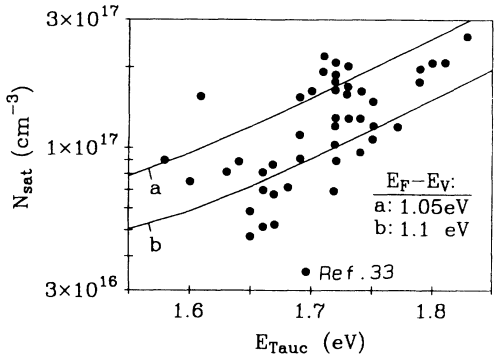

FIG. 10. Calculated and experimental dependence of N_{sat} on band gap. Calculated lines a, b for various positions of E_F.

tal N_{sat}, has been assumed. The three lines indicated a, b, and c here and in the following figures are calculated for different positions of E_F at 0.7, 0.75, and 0.8 eV below E_c, and corresponding positions of D^+ at 0.55 ± 0.05 eV and D^- at 0.95 ± 0.05 eV below E_c. It should be emphasized that the model contains no free parameters. The applied parameters kT_v, N_{v0}, N_H, and E_g are typical for low defect a-Si:H. Modifications of these input parameters have little influence on these results, as shown in more detail below, and uncertainties in capture rates affect the calculated N_{sat} only marginally [see Eq. (33)]. Both the slope of the calculated lines, in agreement with the above estimate, and the absolute value reflect the trend observed experimentally. On the other hand, using the reactions with $i=0$ or 1 Si-H bonds yield smaller N_{sat} ($<10^{16}$ cm^{-3}) than observed as well as larger slopes for $\log_{10}N_{sat}$ vs E_g, indicating that the reaction with two Si-H bonds is the appropriate one.

Varying the hydrogen content has a comparatively small effect on N_{sat}, at least for $c_H > 2\%$. The calculated curves are shown in Fig. 11. The changes with c_H are due to the extra entropy introduced by the Si-H bonds which is only a logarithmic function of c_H. In comparison, the changes with E_g are due to the associated changes of equilibrium carrier densities, which depend exponentially on E_g, explaining the strong dependence of N_{sat} on E_g.

These results suggest that the apparent improvement of a-Si:H by lowering the hydrogen content may be primarily an electronic effect, due to the associated change in band gap. The generally observed improvement of stability for a-SiGe:H alloys and lower stability with carbon alloying may also reflect the associated changes in band gap.

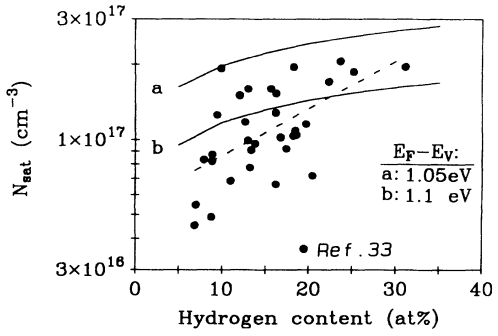

FIG. 11. Calculated and experimental dependence of N_{sat} on hydrogen content.

E. Dependence on generation rate

The dependence of N_{sat} on G together with some data from the literature are shown in Fig. 12. The calculated lines are for room temperature and yield a power law, $N_{sat}\sim G^{\lambda}$ with $\lambda\sim0.27$. But degradation at other temperatures yields very similar results, in accordance with the above estimate, that yields $\lambda=0.27-0.31$ for $T=30-150$°C. For $i=0$ and 1, Eq. (32) yields $\lambda\sim0.37$ and 0.31, respectively, and $N_{sat}<10^{16}$ cm^{-3}. Experimental data show large scatters of λ between 0.15 and 0.35. Again, the agreement with data regarding the power exponent and absolute density is best for $i=2$. The observed "saturation" and the rather small dependence of N_{sat} on light intensity is reproduced without requiring depletion of available defect sites.[38]

In this context it is interesting to note that data from pulsed light soaking[39] show somewhat larger slopes, $N_{sat}\sim G^{0.4}$. For light pulses shorter than the recombination time, the initial free carrier density is $n(0)=p(0)\propto G$, and independent of the defect density. In this case Eq. (31) becomes

$$N_{sat}\sim\left[\frac{np}{n_0p_0}\right]^{\rho T/2T_v}\sim\left[G\exp\left[\frac{E_g}{2kT}\right]\right]^{\rho T/T_v}\sim G^{\lambda_p},$$

where $\lambda_p=\rho T/T_v=0.37-0.42$ at $T=30-105$°C, in good agreement with the experimental slope. Figure 13 shows the data and calculated lines. We note that not only the dependence on generation rate but also the change with

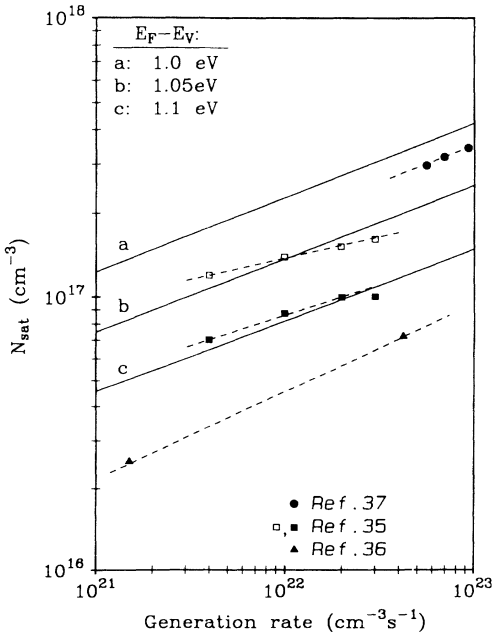

FIG. 12. Calculated and experimental dependence of N_{sat} on generation rate for CW illumination.

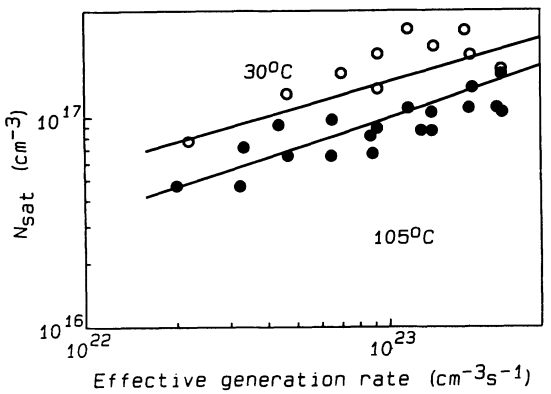

FIG. 13. Calculated and experimental dependence of N_{sat} on effective generation rate for pulse light soaking. Data from Ref. 39. In addition to the standard parameters (Table I) we use the effective carrier density $n_{eff}=n(0)v_{rep}\tau_p$ introduced in Ref. 39 to scale the horizontal axis, where v_{rep} is the laser pulse repetition rate and t_p is the carrier lifetime.

temperature is reproduced quite well with a single set of parameters.

F. Temperature dependence

In Fig. 14 the calculated temperature dependence of N_{sat} and N_0 is compared with experimental data. The single set of parameters used before produces both N_{sat} and N_0 in very good agreement with experiment regarding the absolute values as well as the temperature dependence. The calculated N_0 shows thermally activated behavior with an apparent activation energy of ~ 0.3 eV. This value is rather small compared to the average reaction enthalpy $\Delta H=2(E_D-E_t)\sim 0.9$ eV and is a result of the distribution of ΔH's. The calculated N_{sat} shows very little dependence on the degradation temperature, having a small negative slope dependent on the exact values of the input parameters. The small temperature dependence appears to be in agreement with the displayed data sets as well as most other studies[40,41] that show typical changes by a factor 2 or smaller over the observed temperature ranges, corresponding to activation energies of ~ 0.1 eV or smaller. $N_{sat}(T)$ may be expressed as

$$N_{sat}(T)\sim N_{eq}(T)\left[\frac{G}{\sqrt{c_n c_p}}\exp\left[\frac{E_g}{2kT}\right]\right]^{1/(+T_v/\rho T)} \tag{33}$$

[see Eq. (32)]. The second term obeys a negative temperature dependence primarily due to thermal activation of n_0p_0. With the standard set of input parameters, this term approximately cancels the positive temperature dependence of N_{eq} and so produces a nearly constant N_{sat}. This result is coincidental. Different slopes for $N_{eq}(T)$ will directly affect the slope of $N_{sat}(T)$, which is the reason for the small changes in slopes seen in Fig. 14. However, changing the input parameters within reasonable limits, we were not able to produce larger changes in the resulting slopes for $N_{sat}(T)$. Of course, implicit temperature dependencies, for instance, of the capture rates, kT_v, or E_g, or application of a more detailed recombination model that yields n and p as a function of T,[17] may further affect the results. Given these uncertainties, the actual agreement with the data is remarkably good.

G. Dependence on valence-band tail slope

Figure 15 plots calculated and experimental N_{eq} and N_{sat} as a function of the tail slope kT_v, again using the

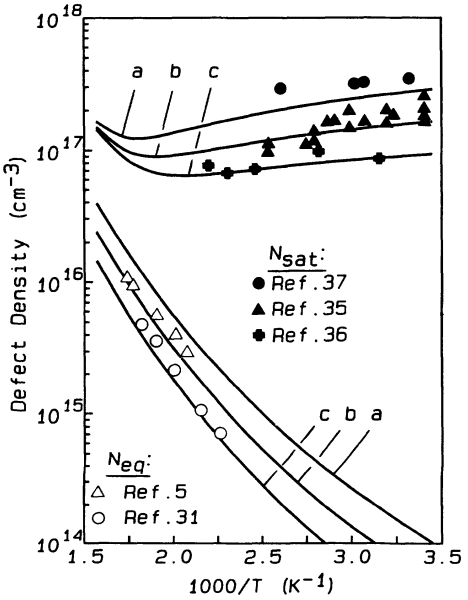

FIG. 14. Calculated and experimental temperature dependence of N_{sat} and N_{eq} in undoped a-Si:H.

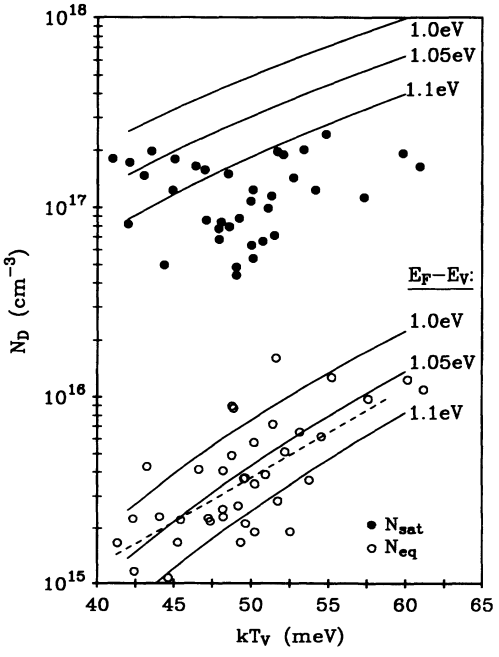

FIG. 15. Calculated and experimental dependence of N_{sat} and N_{eq} on valence-band tail.

standard set of input parameters noted above. Large scatters in the experimental data make correlations difficult to observe. Regarding N_{eq}, the least-squares fit to the experimental data (dashed line) is in good agreement with the calculations and, in fact, other data up to over $kT_v \sim 100$ meV (Ref. 32) follow these lines. While the calculations show also an increase in N_{sat} with kT_v, no apparent correlation is seen experimentally. It should be noted, however, that it is not possible to change kT_v independent of other characteristic parameters that may influence N_{sat}. A smaller band gap or additional recombination paths through broader band tails, for instance, would serve to decrease N_{sat} towards larger kT_v.

IV. DISCUSSION

By combining electronic occupation statistics with the chemical reactions that drive defect formation, it was explicitly shown that the *equilibrated* defect structure of *a*-Si:H does not depend on the type and number of electronic carriers (*e*, *h*, *e*-*h* pairs) involved in the chemical reaction, a result which in fact is required by detailed balance. Therefore one single reaction may be used to derive the defect structure of undoped, *n*-, and *p*-type *a*-Si:H. The resulting structure, however, depends on the type and details of the chemical reaction. The extra entropy of Si-H bonds, for instance, serves to increase the defect density, and the position of the defect bands depends among other things on whether the defects are created in pairs, and whether the two defects are created at the same or statistically independent energy positions.

The energy distribution of equilibrium defect states is primarily determined by the statistical distribution of available defect sites, the effective correlation energy of the defect states, and additional terms entering the reaction enthalpy such as the energy distribution of precursor sites. Energy minimization by a chemical reaction in combination with electronic reoccupation always and generally leads to the formation of two charged defect bands in addition to the band of neutral defect states. This result is based on first principles and does not depend on the specific reaction or model involved. While in the WB-DB conversion model the defect bands are separated by $\sigma^2/2kT_v$ or σ^2/kT_v, other models, for instance, assuming fixed formation energies for the neutral DB, will yield a similar result, the separation being σ^2/kT, where T is the freeze-in temperature.[25] With reasonable parameters for $U=0.1-0.4$ eV and corresponding σ's to maintain the energetic positions of defect bands known in doped material, the overwhelming tendency in equilibrated undoped *a*-Si:H is to produce charged defect states in excess of the neutral defects, in spite of a positive correlation energy, and independent of a particular model for the defect reaction.

While the equilibrium defect structure does not depend on the type and number of carriers involved in the conversion process, metastable defect structures are strongly affected by them. A case study of the three basic reactions, $e+\mathrm{WB}\rightleftharpoons D^-$, $h+\mathrm{WB}\rightleftharpoons D^+$, and $e+h+\mathrm{WB}\rightleftharpoons D^0$ (extended by Si-H bonds) showed that the reactions involving single carriers produced metastable steady-state defect densities and distributions that are incompatible with experimentally observed light-induced defect structures, and only the reaction involving *e*-*h* pairs yields results in agreement with experiment.

Within the WB-DB model, only the reaction involving two Si-H bonds, $e+h+2(\mathrm{Si-H})+\mathrm{WB}\rightleftharpoons D^0+(\mathrm{SiHHSi})$, gave defect densities in agreement with experiment and therefore has been studied in detail. A single set of structural parameters, kT_v, N_{v0}, c_H, E_F, U, and σ, all of which are known experimentally with sufficient accuracy, has been used to calculate the equilibrated and saturated defect structures, $D_{eq}(E)$ and $D_{sat}(E)$, with no free parameters involved. The dependence of equilibrium and saturated defect densities on external conditions T, and G, and changes in structural parameters E_g, c_H, and kT_v has been investigated. Given the principal simplicity of the model, i.e., a homogeneous soup of chemical bonds, which are related by the law of mass action and electronic occupancy and in nonequilibrium manipulated by changes in free carrier densities and occupation functions, it is perhaps surprising how well virtually all experimental observations regarding equilibrium and metastable steady-state defect structures are reproduced by this single reaction with a single set of parameters.

A very important implication of chemical equilibration in combination with occupation statistics is the change of the defect *distribution* with light soaking, predicting a larger increase of the neutral defect states as compared to the charged defect bands. Again, this result is based on first principles, and does not depend on the specific model or reaction applied nor on the exact model parameters. Experimental evidence for such a behavior is found, apart from subgap absorption vs spin density, in light-induced electron spin resonance measurements.[42,43] A further implication of occupancy statistics on defect distributions is an intrinsic shift of the dark Fermi level with light soaking, which is a well-known feature of light soaking and in the framework of this model caused by asymmetries in capture rates and free carrier concentrations during light soaking.

The model so far has been limited to steady-state defect reactions, which do not necessarily require a knowledge of the kinetic barriers. A few straightforward implications on the associated defect kinetics, however, are probably worth mentioning. Because from first principles, in equilibrium the results for the reaction $e+h+\mathrm{WB}\rightleftharpoons D^0$ are identical to those from $\mathrm{WB}\rightleftharpoons D^0$ (see Sec. II B), it is easy to show that such a reaction in nonequilibrium steady state implies a rate equation of the form

$$\frac{dN_D}{dt} = A\frac{np}{n_0p_0}(N_t-N_D)-BN_{D^0}=0 \ ,$$

where A and B are the forward and backward rate coefficients with kinetic barriers $E_A=E^*-E_t$ and $E_B=E^*-E_D$. (See also Appendix B.) It is important to note that the forward rate is not determined by the *np* product, but rather by the deviation of the *np* product from equilibrium, np/n_0p_0. This is a direct result of the chemical reaction assumed above and must be generally valid, if the equilibrium defect structure is to be viewed as a special case of metastable steady-state defect structures.

The forward rate is consistent with the $t^{1/3}$ defect kinetics[40] where the Staebler-Wronski prefactor is $c_{SW}=A/n_0p_0$. The backward reaction in its present form does not explicitly include an optical or carrier-induced anneal term. However, because the reaction is mediated by H motion, the rate coefficients A and B themselves are expected to be correlated to the hydrogen kinetics, which is known to be carrier dependent.[44] This dependence may account for an accelerated defect kinetics towards steady state under light,[37] carrier injection,[45] or doping.[1] If the barrier E^* between defect and weak-bond configurations depends on n or p, which should be the case for a kinetic barrier due to H motion, both A and B have the same dependence on n (or p) and the steady-state solution of the rate equation, of course, is not affected by these additions. This is a very important feature of this model, because it allows one to decouple the defect kinetics from the steady-state or saturation values without requiring complete depletion of defect formation sites.

It should be stressed that while the equilibrated defect density N_{eq} shows a clear thermal activation of ~ 0.3 eV, the calculated temperature dependence of N_{sat} turned out to be very small, although the anneal (backward) reaction does not include explicitly any free carriers. With a thermal activation of the backward rate coefficient inferred from annealing of light-induced defects, $E_B \sim 1.1$ eV,[40] the activation energy of the forward rate is $E_A=E_B+(E_D-E_t)\sim 1.5-1.8$ eV. Under illumination, however, the forward rate is $A(np/n_0p_0)$ where np/n_0p_0 has a negative temperature dependence. It serves to increase the forward rate and to decrease its temperature dependence. With the differential treatment, it turns out that the temperature dependence of the forward and backward rates approximately cancels, producing a nearly temperature-independent $N_{sat}(T)$. This result is coincidental, and variations in structural parameters such as band gap, tail slope, or the position of E_F and therefore the defects, will slightly affect the temperature dependence, producing small changes in activation energies for $N_{sat}(T)$. The inclusion of the *ratio*, np/n_0p_0, instead of the np product alone, is crucial to the present results. In such a case, no explicit optical anneal term[46] is required to obtain N_{sat} nearly independent of temperature. The differential treatment also reproduces the observed sublinear dependence of N_{sat} on the generation rate as well as the difference between cw and pulsed light soaking requiring no depletion of defect formation sites.[38]

A further direct implication of the discussed steady-state model is a nearly temperature-independent defect creation rate, in spite of a large forward barrier $E_A \sim 1.5-1.8$ eV in the dark. The Staebler-Wronski factor is $c_{SW}\sim A/n_0p_0\sim\exp[E_g-E_A/kT]$ with an activation energy E_g-E_A which may be rather small, in agreement with experiment.[40] A further refinement of the kinetics may account for the expected distribution of barrier energies E_A, related to the distributions of bonding energies of the precursors that are converted to defects. A dispersive model with an exponential barrier distribution of slope kT_v has been suggested,[47] which in the present context yields for the forward rate

$$\frac{dN_D}{dt}\sim\frac{A/n_0p_0}{N_D^{T_v/T-1}}np\sim\left[\frac{A}{n_0p_0}\right]^{T/T_v}np^{T/T_v}t^{T/T_v-1}$$

and therefore for the effective Staebler-Wronski prefactor $c_{SW}^*\sim[A/n_0p_0]^{T/T_v}\sim\exp[E_g-E_A/kT_v]$, independent of temperature for any value of E_A. [The small temperature dependence of $N_D(t)$ seen experimentally is now included and well described by the other factors, $np^{T/T_v}t^{T/T_v-1}$]. Yet, c_{SW} retains the dependence on band gap, according to $d(\ln c_{SW})/dE_g=kT_v^{-1}$, in general agreement with the observation that samples of lower band gap tend to have slower degradation rates.[48]

V. CONCLUSIONS

In summary, we have derived an analytical expression valid both for the equilibrium and for the metastable steady-state defect density of states in a-Si:H under general nonequilibrium conditions. Key ingredients to the model are (i) a chemical equilibration reaction between weak bonds and dangling bonds mediated by H motion, (ii) a differential treatment of the reaction accounting for the distribution of weak-bond and available dangling-bond energies, (iii) electronic occupancy of the equilibrating defect structure according to occupation statistics, and (iv) e-h pair recombination driving the forward reaction.

The derived expression is determined entirely by inherent, experimentally accessible, structural properties of a-Si:H such as the tail slope, band gap, hydrogen content, correlation energy, and amorphous broadening of defect bands, as well as by the external conditions, temperature, and imposed free carrier concentrations. The model contains no free parameters. It predicts an excess of charged defect states in annealed a-Si:H, and a change in the defect distribution with a reduction of the ratio of charged-to-neutral defects by light soaking. All dependencies of equilibrated and saturated defect densities and distributions on external conditions such as equilibration/degradation temperature and generation rate, and on sample variations such as band gap, hydrogen content, and tail slope, are in excellent agreement with experimental data using the reaction $e+h+2(\text{Si-H})+\text{WB}\rightleftharpoons 2D^0+(\text{SiHHSi})$ and a single set of parameters which is typical for low defect a-Si:H.

Implications of the steady-state model on the defect kinetics have been discussed and found to be in general agreement with observations. In particular, it was shown from first principles that the saturated defect density and defect creation rate must contain the *deviation* of np products from the equilibrium value n_0p_0 rather than the np product alone. This fact resolves a number of open questions regarding defect saturation and defect kinetics, providing, for instance, a direct explanation of features such as nearly temperature-independent saturation defect densities and defect kinetics with light soaking in spite of a strong thermal activation of these quantities in the dark, or the apparent correlation of saturation defect densities with band gap.

ACKNOWLEDGMENTS

I thank Warren Jackson and Bob Street for many invaluable discussions and critical reading of the manuscript. Support by NREL under Contract No. HG-1-10063-9 is gratefully acknowledged.

APPENDIX A

The close correlation found between hydrogen diffusion and defect kinetics insinuates the involvement of one or more Si:H bonds in the defect formation. The following reaction with $i=1$ Si-H bond:[4,49]

$$\text{Si-H}+\text{WB}\rightleftarrows D_1+(\text{Si-H}|D_2)\ , \tag{A1}$$

$$(\text{Si-H}|\text{Si-H})+\text{WB}\rightleftarrows(\text{Si-H}|D_1)+(\text{Si-H}|D_2)\ , \tag{A2}$$

or with $i=2$ Si-H bonds:[4,5]

$$2\text{Si-H}+\text{WB}\rightleftarrows(\text{Si-H}|\text{Si-H})+D_1+D_2 \tag{A3}$$

have been suggested. Applying the appropriate laws of mass action and solving for the gap-state density $D(E)$, we briefly show that all reactions yield the same spectral shape for $D(E)$ as in Eq. (20), the only difference being the scaling factor γ. Noting that in Eq. (A3) $[\text{Si-H}|\text{Si-H}]=[D_1]$ (or $=[D_2]$), and with $N_{D,\text{pair}}=N_{D1}=N_{D2}$, we may write a generalized law of mass action for $i=0$, 1, or 2 Si-H bonds involved:

$$\frac{(N_{D1})^i N_{D2}}{(N_{\text{H}})^i(N_t-N_{D2})}=\frac{2}{f^0(E_1)}\frac{2}{f^0(E_2)}\times\exp\left[-\frac{E_1+E_2-2E_t}{kT}\right]\ . \tag{A4}$$

Because of the assumed symmetry, the subscripts 1 and 2 of course may be interchanged. In the case of an energetic distribution of weak bonds and defect sites we have in addition to Eq. (18)

$$\frac{d^3N_{D1}}{d^3N_{\text{H}}}=\frac{D_1(E_1)}{N_{\text{H}}P(E_1)}$$

and, with $D(E)=2D_1(E)=2D_2(E)$, in analogy to Sec. II B,

$$D(E_2)=2\int\int\frac{g(E_t)P(E_1)P(E_2)}{1+\left[\frac{D(E_1)}{2N_{\text{H}}P(E_1)}\right]^i\frac{f^0(E_1)}{2}\frac{f^0(E_2)}{2}\exp\left[\frac{\Delta G}{kt}\right]}dE_t dE_1\ . \tag{A5}$$

Equation (A5) is essentially identical to Eq. (19) except for the term in square brackets which is due to the extra entropy introduced by the hydrogen. For integration limits $E_1, E_t=-\infty,\ldots,+\infty$, Eq. (A5) has an analytical solution for $D(E)$, and we find the same energy distribution as without hydrogen involvement,

$$D(E)=\gamma_i P(E+\sigma^2/2kT_v)(2/f^0)^{T/2T_v}\ ,$$

but now with a generalized scaling factor γ_i,

$$\gamma_i=[2N_{v0}\alpha\beta]^{\rho}[2N_{\text{H}}]^{1-\rho}\delta\ , \tag{A6}$$

where

$$\alpha=\frac{\pi kT}{2\sin(\pi T/2T_v)}\ , \tag{A7}$$

$$\beta=\int P(E)\left[\frac{2}{f^0}\exp-\frac{E}{kT}\right]^{(T/2T_v)(1-iT/2T_v)}dE\ , \tag{A8}$$

$$\sigma=\exp\left[\frac{\sigma^2}{2(2kT_v)^2}-\frac{E_p-E_v}{2kT_v}\right]\ , \tag{A9}$$

and $\rho=(1+iT/2T_v)^{-1}$.[50]

APPENDIX B

An appropriate treatment of nonequilibrium steady state requires application of rate equations rather than the law of mass action. In equilibrium, the law of mass action may be derived from the rate equations as a special case. Under nonequilibrium, the principle of detailed balance does not apply. In general, one may have a number of competing reactions. As conversion rates depend exponentially on barrier heights, frequently the reaction with the highest conversion rates (lowest-energy barriers) will determine the resulting steady state. In such a case an approximate expression is obtained which is equivalent to the law of mass action for this reaction.

To illustrate this point, consider the three representative simplified reactions $e+\text{WB}\rightleftarrows D^-$, $h+\text{WB}\rightleftarrows D^+$, and $e+h+\text{WB}\rightleftarrows D^0$. The rate equation for the three reactions is

$$\begin{aligned}dN_D/dt=&A_1 n(N_t-N_D)-B_1 f^- N_D\\&+A_2 p(N_t-N_D)-B_2 f^+ N_D\\&+A_3 np(N_t-N_D)-B_3 f^0 N_D\ ,\end{aligned} \tag{B1}$$

with the forward and backward rate coefficients

$$A_i=v_i\exp\left[-\frac{E_i^*-E_{\text{WB}}}{kT}\right]\ ,\quad B_i=v_i\exp\left[-\frac{E_i^*-E_{B,i}}{kT}\right]\ . \tag{B2}$$

(For a correct solution, the prefactors must be multiplied by the appropriate degeneracy factors. To allow for kinetic effects such as light- or current-induced recovery, the barriers E_i^* may be carrier dependent.)

In equilibrium, detailed balance applies. The three

lines in (B1) must each be $\equiv 0$ independently, and therefore

$$\frac{N_D}{N_t - N_D} = \frac{1}{f^-}\frac{n_0 A_1}{B_1} = \frac{1}{f^+}\frac{p_0 A_2}{B_2} = \frac{1}{f^0}\frac{n_0 p_0 A_3}{B_3} . \tag{B3}$$

For the ratios A_i/B_i the prefactors ν_i and barrier energies E_i^* cancel, and essentially the laws of mass action derived in Sec. II A are recovered.

On the other hand, under nonequilibrium steady state, only the sum of the three lines is $\equiv 0$, and Eq. (B1) gives

$$\frac{N_D}{N_t - N_D} = \frac{n A_1 + p A_2 + np A_3}{f^{-*} B_1 + f^{+*} B_2 + f^{0*} B_3} . \tag{B4}$$

In general, Eq. (B4) can only be solved with knowledge of the various rate coefficients. If, however, the rates of one reaction are much higher than for the other reactions, Eq. (B4) reduces to the respective expression in Eq. (B3), only with equilibrium carrier densities and occupation functions replaced by the nonequilibrium ones. In this case, the nonequilibrium steady state may be solved without knowledge of the rate constants by the law of mass action associated with this reaction. Differential treatment yields the solutions for the metastable defect structure, such as Eq. (24) or (25).

---

*Present address: Zentrum für Sonnenenergie- und Wasserstoff-Forschung, Hessbruehlstrasse 21C, 70565 Stuttgart, Germany.

[1]R. A. Street, J. Kakalios, and T. M. Hayes, Phys. Rev. B **34**, 3030 (1986).

[2]Z. Smith *et al.*, Phys. Rev. Lett. **57**, 2450 (1986); Z. Smith and S. Wagner, in *Advances in Amorphous Semiconductors,* edited by H. Fritzsche (World Scientific, Singapore, 1989), p. 469.

[3]T. J. McMahon and R. Tsu, Appl. Phys. Lett. **55**, 412 (1987).

[4]R. A. Street and K. Winer, Phys. Rev. B **40**, 6236 (1989).

[5]S. Zafar and E. A. Schiff, Phys. Rev. B **40**, 5235 (1989); Phys. Rev. Lett. **66**, 1493 (1991).

[6]Y. Bar-Yam, D. Adler, and J. D. Joannopoulos, Phys. Rev. Lett. **57**, 467 (1986).

[7]K. Pierz, W. Fuhs, and H. Mell, Philos. Mag. B **63**, 123 (1991).

[8]K. Winer, Phys. Rev. B **41**, 12 150 (1990).

[9]G. Schumm and G. H. Bauer, Philos. Mag. B **64**, 515 (1991).

[10]G. Schumm and G. H. Bauer, J. Non-Cryst. Solids **137/138**, 315 (1991).

[11]G. Schumm and G. H. Bauer, in *Conference Record of the 22nd IEEE Photovoltaic Specialists Conference* (IEEE, New York, 1991), p. 1225.

[12]S. C. Deane and M. J. Powell, Phys. Rev. Lett. **70**, 1654 (1993).

[13]In this particular reaction, the two DB's must be an intimate pair. Allowing them to diffuse away from the broken WB and stabilize at other positions in the network requires the involvement of additional bonds, with associated reactions such as Si-Si+WB$\rightleftharpoons D_1 + D_2$ or Si-H+WB$\rightleftharpoons D_1 + D_2$. The first reaction requires massive structural reconfigurations by floating bonds, the second, more realistic, reaction is discussed in Appendix A.

[14]H. Okamoto and Y. Hamakawa, Solid State Commun. **24**, 23 (1977).

[15]M. Lannoo and J. Bourgoin, in *Point Defects in Semiconductors I,* edited by M. Cardona, P. Fulde, and H.-J. Queisser, Springer Series in Solid State Sciences Vol. 22 (Springer, Berlin, 1981), p. 195.

[16]To be formally correct in the expression for the entropy ΔS, the effective density of states N_c should be multiplied by the volume considered. In that case, by doing the same for the densities of electrons, WB's, and DB's in Eq. (11), the solution Eq. (14) will not be affected.

[17]F. Vaillant and D. Jousse, Phys. Rev. B **34**, 4088 (1986).

[18]R. A. Street and D. K. Biegelsen, Solid State Commun. **33**, 1159 (1980).

[19]L. Chen, J. Tauc, J. Kocka, and J. Stuchlik, Phys. Rev. B **46**, 2050 (1992).

[20]J. Kocka, M. Vanecek, and F. Schauer, J. Non-Cryst. Solids **97&98**, 715 (1987).

[21]P. G. LeComber and W. E. Spear, Philos. Mag. Lett. B **53**, L1 (1986).

[22]T. J. McMahon and J. P. Xi, Phys. Rev. B **34**, 2475 (1986).

[23]G. Schumm, C.-D. Abel, and G. H. Bauer, J. Non-Cryst. Solids **137/138**, 351 (1991).

[24]H. M. Branz and M. Silver, Phys. Rev. B **42**, 7420 (1990).

[25]Y. Bar-Yam and J. D. Joannopoulos, J. Non-Cryst. Solids **97/98**, 467 (1987).

[26]A. Doghmane and W. E. Spear, Philos. Mag. B **53**, 463 (1986).

[27]J. Kocka, C. E. Nebel, and C.-D. Abel, Philos. Mag. B **63**, 221 (1991).

[28]G. Schumm, E. Lotter, and G. H. Bauer, Appl. Phys. Lett. **60**, 3262 (1992).

[29]M. S. Brandt, A. Asano, and M. Stutzmann, in *Amorphous Silicon Technology-1993,* edited by E. A. Schiff, M. J. Thompson, A. Madan, K. Tanaka, and P. G. LeComber, MRS Symposia Proceedings No. 297 (Materials Research Society, Pittsburgh, 1993).

[30]W. den Boer, M. J. Geerts, M. Ondris, and H. M. Wentinck, J. Non-Cryst. Solids **66**, 363 (1984).

[31]T. J. McMahon, Sol. Cells **30**, 235 (1991).

[32]M. Stutzmann, Philos. Mag. B **60**, 531 (1989).

[33]M. Isomura, X. Xu, and S. Wagner, Sol. Cells **30**, 177 (1991).

[34]A. H. Mahan and M. Vanecek, in *Amorphous Silicon Materials and Solar Cells,* edited by Byron L. Stafford, AIP Conf. Proc. No. 234 (AIP, New York, 1991), p. 195.

[35]M. Isomura, N. Hata, and S. Wagner, J. Non-Cryst. Solids **137/138**, 223 (1991).

[36]P. V. Santos, W. B. Jackson, and R. A. Street, Phys. Rev. B **44**, 12 800 (1991).

[37]Z. Y. Wu, J. M. Siefert, and B. Equer, J. Non-Cryst. Solids **137/138**, 227 (1991).

[38]D. Redfield, Appl. Phys. Lett. **48**, 846 (1986).

[39]N. Hata, G. Ganguly, S. Wagner, and A. Matsuda, Appl. Phys. Lett. **61**, 1817 (1992).

[40]M. Stutzmann, W. B. Jackson, and C. C. Tsai, Phys. Rev. B **32**, 23 (1985).

[41]M. Grimberger, L. E. Benatar, A. Fahrenbruch, A. Lopez-Otero, D. Redfield, and R. H. Bube, in *Amorphous Silicon Materials and Solar Cells* (Ref. 34), p. 138.

[42]T. Shimizu, H. Kidoh, A. Morimoto, and M. Kumeda, Jpn. J. Appl. Phys. **28**, 586 (1989).
[43]G. Schumm, W. B. Jackson, and R. A. Street, Phys. Rev. B **48**, 14 198 (1993).
[44]P. V. Santos, N. M. Johnson, R. A. Street, M. Hack, R. Thompson, and C. C. Tsai, Phys. Rev. B **47**, 10 244 (1993).
[45]R. A. Street and M. Hack, J. Non-Cryst. Solids **137/138**, 263 (1991).
[46]D. Redfield, Appl. Phys. Lett. **52**, 492 (1988).
[47]P. V. Santos and W. B. Jackson, Phys. Rev. B **44**, 10 937 (1991); J. Non-Cryst. Solids **137/138**, 202 (1991).
[48]G. Schumm, C.-D. Abel, and G. H. Bauer, in *Amorphous Silicon Technology-1992,* edited by M. J. Thompson, Y. Hamakawa, P. G. LeComber, A. Madan, and E. A. Schiff, MRS Symposia Proceedings No. 258 (Materials Research Society, Pittsburgh, 1992), p. 505.
[49]W. B. Jackson, Phys. Rev. B **41**, 10 257 (1990).
[50]Equation (A5) and the resulting prefactor γ_i are very similar to an expression recently obtained by an equivalent approach using a generalized defect chemical potential (Ref. 12). Deane and Powell suggested that the correct treatment of the equilibrium reactions would be to assume identical energy positions for the pair of formed DB's, in which case Eq. (A5) would reduce to a simpler form equivalent to their Eq. (10). They claim the use of statistical independent energy positions E_1 and E_2, as we have done, would apply only for intimately coupled pairs of defects. This is not the case. It applies in general to all defects that are producd in pairs at independent energy positions, because detailed balance requires the equilibration between each subset of DB's at E_1, DB's at E_2, and WB's at E_t, independent of whether the two DB's formed can diffuse apart. It can be shown that only a reaction where the two DB's are produced by breaking two independent WB's (most simple case: $WB_1+WB_2 \rightleftharpoons D_1+D_2$) may be reduced to the simple form of Ref. 12. Such a reaction may apply for a global equilibration between all WB's and DB's, but not for a more localized equilibration where DB's are not likely to diffuse over large distances (more than the average spacing of ~ 30 nm between DB's). In any case, both approaches yield qualitatively similar results, with only minor quantitative differences regarding the spectral shape and total defect density.